Monitoring of Three-Phase Signals based on Singular-Value Decomposition

V. Choqueuse, *Member, IEEE,* P. Granjon, A. Belouchrani, *Senior Member, IEEE,* F. Auger, *Senior Member, IEEE,* and M. Benbouzid, *Senior Member, IEEE,*

Abstract—In this paper, a new approach for the analysis of three-phase electrical signals is considered. While most of the existing techniques are based on fixed transforms such as the Clarke transform, this paper investigates the use of a data-driven approach called the Singular Value Decomposition (SVD). As compared to other transforms, this study shows that the SVD has the distinct advantage of clearly separating the contributions of the phasor configuration and signal instantaneous parameters. Under additive white Gaussian noise, this paper also describes several algorithms based on the SVD for signal monitoring. The first algorithm can detect unbalanced systems and classify them into two categories: system with an off-nominal subspace and systems with ellipticity. The second algorithm can estimate the angular frequency based on the periodogram of the right singular vectors. As compared to other existing approaches, simulations show that the proposed techniques give a good compromise between computational complexity and statistical performance.

Index Terms—Three-phase signals, Singular-Value Decomposition, Generalized Likelihood Ratio Test, Frequency Estimation.

I. INTRODUCTION

Three-phase electrical signals play a key role in power electronic applications at the generation, transmission and distribution side. Under nominal conditions, each phase signal has a sinusoidal shape with a constant magnitude and a fundamental frequency equal to 60Hz (or 50Hz) [1], [2]. Moreover, balanced three-phase signals have equal magnitude and are ideally $2\pi/3$ apart in terms of phase angles. In practice, three-phase signals are seldom stationary and the phasor configuration may deviate significantly from the balanced case [3]. In a smart grid, these deviations are monitored using synchronized devices called Phasor Measurement Units (PMU) [4]–[6]. In particular, two signal parameters are of main interest: the signal fundamental frequency [7]–[10] and the phasor configuration [11], [12]. This has motivated the development of new low-complexity algorithms for frequency estimation and unbalanced detection in PMU devices.

Numerous studies have addressed the frequency estimation problem for electrical signals [6]. A commonly used approach for frequency estimation is based on the Discrete Time Fourier Transform (DTFT) [13], [14] and its extension such as the Interpolated Discrete Fourier Transform (IpDFT) [15]–[17]. Nevertheless, as recently pointed out in [18], these single-phase techniques usually require a large number of cycles and Signal to Noise Ratio (SNR) to meet the requirements of the IEEE Standard C37.118-2011 dealing with PMU specifications. To improve the estimator performance, one possible solution is to exploit the multi-dimensional nature of three-phase signals. For balanced signals, a conventional approach is based on the Clarke transform [19], [20]. After Clarke transform, the so-called $\alpha\beta$ components can be further processed to estimate the signal frequency [7], [8], [21]–[25] and other parameters of interest [23], [25]. For unbalanced signals, several authors have also investigated the use of the $\alpha\beta$ components for frequency estimation [7], [24]. However, this strategy has two major drawbacks. First, under unbalanced conditions, the use of the $\alpha\beta$ components usually requires sophisticated approaches since the signal trajectory depends both on the phasors configuration and on the signal instantaneous parameters. Then, while the Clarke transform is perfectly well-suited for the analysis of balanced three-phase signals, this technique is inherently suboptimal under unbalanced conditions [10]. Departing from this approach, some authors have also investigated the use of a data-driven approach called the Principal Component Analysis (PCA) for signal analysis [10], [23]. As compared to the Clarke transform, the PCA has the distinct advantage of extracting two orthogonal components directly from the covariance matrix of the multi-dimensional signal whatever the unbalance configuration [26].

Regarding the unbalance detection problem, conventional approaches are based on the computation of the voltage unbalance factors [27] or the analysis of the $\alpha\beta$ components [28]. To improve the detection performance, some authors have investigated the use of parametric approaches. These include the Generalized Likelihood Ratio Test (GLRT) [29], the Generalized Locally Most Powerful Test (GLMP) [30], or Information Theoretical Criteria techniques [31], [32]. While these techniques are based on the raw three-phase signal, a GLRT-based approach has also been proposed for the challenging case where only the native PMU outputs are available for detection purpose [33]. As compared to non-parametric approaches, parametric techniques have better statistical performance but are less robust to model mismatch. In particular, theses parametric detectors assume perfectly sine-wave signals and their performance degrades quickly in the presence of time-varying amplitude and/or frequency.

In this paper, we propose a new approach for the analysis of

V. Choqueuse is with the Lab-STICC, UMR CNRS 6285, ENIB, 29280 Plouzané (e-mail: choqueuse@enib.fr). P. Granjon is with the GIPSA-lab, UMR CNRS 5216, Grenoble INP, 38402 Saint Martin D'Heres, France (e-mail:pierre.granjon@gipsa-lab.grenoble-inp.fr). A. Belouchrani is with the Electrical Engineering Department., Ecole Nationale Polytechnique, Algiers 16200, Algeria (e-mail: adel.belouchrani@enp.edu.dz). F. Auger is with the IREENA, LUNAM, 44606 Saint-Nazaire, France (e-mail: francois.auger@univ-nantes.fr). M. Benbouzid is with the IRDL, UMR CNRS 6027 IRDL, University of Brest, 29238 Brest, France (Mohamed.Benbouzid@univ-brest.fr).

three-phase signals based on a Singular-Value Decomposition (SVD). As compared to other multi-dimensional tools such as the Clarke transform or the PCA, the main advantage of the SVD is that it gives a better insight into the structure of the three-phase signal. Specifically, by decomposing the three-phase signal into a product of three matrices, the SVD allows to clearly distinguish between the contribution of the phasors and signal instantaneous parameters. In particular, contrary to the PCA which has been previously used for estimation purpose [10], [23], the proposed technique can be used both for unbalance detection and frequency estimation. In this context, the contribution of this paper is twofold:

- First, we show how the SVD is related to the structure of the three-phase signal.
- Second, under Gaussian noise assumption, we show how to process the SVD to detect different types of off-nominal conditions and to estimate the signal frequency.

The paper is organized as follows. Section II introduces the signal model and the assumptions made in the study. Section III presents the expression of the SVD of the three-phase signal. Section IV shows how to detect off-nominal conditions from the SVD and how to estimate the signal frequency. Finally, Section V reports on the performance of the proposed techniques with simulation signals.

II. SIGNAL MODEL

A. Three-phase Signal Model

Unbalanced three-phase signals can be described under noiseless condition by the following scalar-form model [34]

$$x_k[n] = d_k a[n] \cos(\phi[n] + \varphi_k), \quad (1)$$

where the quantities $a[n]$ and $\phi[n]$ correspond to the instantaneous amplitude and phase respectively, while $d_k \geq 0$ and $\varphi_k \in [0, 2\pi]$ correspond to the scaling factor and initial phase-angle on phase $k = 0, 1, 2$. Using complex notations, the three-phase signal can be expressed more compactly as $z_k[n] = \Re e(c_k z[n])$ where the complex *stationary phasors* c_k ($k = 0, 1, 2$) and the complex signal $z[n]$ are given by

$$c_k \triangleq d_k e^{j\varphi_k} \quad (2a)$$

$$z[n] \triangleq a[n] e^{j\phi[n]}. \quad (2b)$$

In practice, note that three-phase signal can also contains other frequency components such as harmonics or inter-harmonics. In this study, we assume that these high-frequency components have been removed in a pre-processing stage by using a digital low-pass filter[1].

The goal of this study is to analyse the complex phasors c_k and the complex signal $z[n]$ from N samples of the three-phase signal $x_k[n]$ ($k = 0, 1, 2$). By using matrix notations, the three-phase signal of Eq. (1) can be expressed as

$$\mathbf{X} = \mathbf{C}\mathbf{Z}^T, \quad (3)$$

where $(.)^T$ denotes the matrix transpose, and

[1]It should be noted that the use of a digital low-pass filter introduces a phase shift and can increase the computation time.

- $\mathbf{X}$ is a $3 \times N$ matrix which is defined as

$$\mathbf{X} = \begin{bmatrix} x_0[0] & \cdots & x_0[N-1] \\ x_1[0] & \cdots & x_1[N-1] \\ x_2[0] & \cdots & x_2[N-1] \end{bmatrix}, \quad (4)$$

- $\mathbf{Z}$ is a $N \times 2$ matrix containing the real and imaginary parts of the complex signal $z[n]$ and is defined as

$$\mathbf{Z} \triangleq \begin{bmatrix} \Re e(\mathbf{z}) & \Im m(\mathbf{z}) \end{bmatrix}, \quad (5)$$

where $\mathbf{z} \triangleq \begin{bmatrix} z[0] & \cdots & z[N-1] \end{bmatrix}^T$,

- $\mathbf{C}$ is a 3×2 matrix which is defined as

$$\mathbf{C} \triangleq \begin{bmatrix} \Re e(\mathbf{c}) & \Im m(\mathbf{c}^*) \end{bmatrix}, \quad (6)$$

where $(.)^*$ denotes the complex conjugate and $\mathbf{c} \triangleq \begin{bmatrix} c_0 & c_1 & c_2 \end{bmatrix}^T$.

B. Assumptions

In Eq. (1), the signal model cannot by uniquely identified. Indeed, as $x_k[n] = \Re e(c_k z[n])$, it can be easily checked that $x_k[n] = \Re e(c_k^b z^b[n])$ where $c_k^b = \beta c_k$ and $z^b[n] = z[n]/\beta$ with $\beta \in \mathbb{C}^*$. In this study, we assume a particular normalisation on the stationary phasors and complex signal in order to obtain simple expressions for the SVD.

Assumption 1. *The energy of $z[n]$, denoted ϵ_z, is equal to*

$$\epsilon_z \triangleq \mathbf{z}^H \mathbf{z} = \sum_{n=0}^{N-1} |z[n]|^2 = 2. \quad (7)$$

Assumption 2. *The sum of the squared phasors, denoted q_c, is a positive real number i.e. Arg $(q_c) = 0$ where*

$$q_c \triangleq \mathbf{c}^T \mathbf{c} = \sum_{k=0}^{2} c_k^2. \quad (8)$$

It is important to note that these two assumptions are not restrictive. Indeed, it is always possible to preserve the two requirements $\epsilon_z = 2$ and Arg $(q_c) = 0$ by making the substitution $c_k \rightarrow \beta c_k$ and $z[n] \rightarrow z[n]/\beta$ with $\beta = \sqrt{\epsilon_z/2} e^{-j\text{Arg}(q_c)/2}$. To obtain simple expressions for the SVD, we also make the classical assumption that $z[n]$ is an analytic signal, at least asymptotically. Mathematically, a signal is said to be analytic if its Discrete Time Fourier Transform (DTFT), $Z(\omega)$, satisfies [35]

$$Z(\omega) \triangleq \sum_{n=0}^{N-1} z[n] e^{-j\omega n} = 0 \text{ for } -\pi < \omega < 0. \quad (9)$$

By using the Parseval Identity, this assumption implies that

$$q_z \triangleq \sum_{n=0}^{N-1} z^2[n] = \frac{1}{2\pi} \int_{-\pi}^{\pi} Z(\omega) Z(-\omega) d\omega = 0. \quad (10)$$

By using Assumptions 1 and 2 and Eq. (10), we obtain the following proposition.

Proposition 1. *The matrices $\mathbf{Z}^T \mathbf{Z}$ and $\mathbf{C}^T \mathbf{C}$ can be decomposed as*

$$\mathbf{Z}^T \mathbf{Z} = \mathbf{I}_2 \quad (11a)$$

$$\mathbf{C}^T \mathbf{C} = \frac{1}{2} \begin{bmatrix} \epsilon_c + q_c & 0 \\ 0 & \epsilon_c - q_c \end{bmatrix}, \quad (11b)$$

where $\mathbf{I}_2$ is the identity matrix of size 2×2, and $\epsilon_c \triangleq \mathbf{c}^H \mathbf{c} = \sum_{k=0}^{2} |c_k|^2$.

III. SINGULAR-VALUE DECOMPOSITION OF THE THREE-PHASE SIGNAL

As $\mathbf{C}$ in (3) is a 3×2 matrix, the Singular-Value Decomposition of $\mathbf{X}$ presents at most two non-zero singular values. Therefore, the "compact" SVD can be expressed as

$$\mathbf{X} = \mathbf{U}_\mathbf{x} \mathbf{S}_\mathbf{x} \mathbf{V}_\mathbf{x}^T \qquad (12)$$

- $\mathbf{U}_\mathbf{x}$ is a 3×2 semi-orthogonal matrix ($\mathbf{U}_\mathbf{x}^T \mathbf{U}_\mathbf{x} = \mathbf{I}_2$) that contains the left singular vectors of $\mathbf{X}$,
- $\mathbf{S}_\mathbf{x} = \text{diag}(\sigma_2, \sigma_1)$ is a 2×2 diagonal matrix that contains the singular values of $\mathbf{X}$ with $\sigma_2 \geq \sigma_1$,
- $\mathbf{V}_\mathbf{x}$ is a $N \times 2$ semi-orthogonal matrix ($\mathbf{V}_\mathbf{x}^T \mathbf{V}_\mathbf{x} = \mathbf{I}_2$) that contains the right singular vectors of $\mathbf{X}$.

In the following subsections, we show how the SVD matrices are related to the complex phasors c_k and analytic signal $z[n]$.

A. General case

Proposition 2. *Using Proposition 1, the SVD of $\mathbf{X}$ can be expressed as $\mathbf{X} = \mathbf{U}_\mathbf{x} \mathbf{S}_\mathbf{x} \mathbf{V}_\mathbf{x}^T$, where*

$$\mathbf{U}_\mathbf{x} = \mathbf{C} \mathbf{S}_\mathbf{x}^{-1} \qquad (13a)$$

$$\mathbf{S}_\mathbf{x} = \begin{bmatrix} \sqrt{\frac{\epsilon_c + q_c}{2}} & 0 \\ 0 & \sqrt{\frac{\epsilon_c - q_c}{2}} \end{bmatrix} \qquad (13b)$$

$$\mathbf{V}_\mathbf{x} = \mathbf{Z} \qquad (13c)$$

with $\epsilon_c = \sum_{k=0}^{2} |c_k|^2$ and $q_c = \sum_{k=0}^{2} c_k^2$.

Proof. Using Eq. (13a) to (13c), one can check that $\mathbf{U}_\mathbf{x} \mathbf{S}_\mathbf{x} \mathbf{V}_\mathbf{x}^T = \mathbf{C} \mathbf{S}_\mathbf{x}^{-1} \mathbf{S}_\mathbf{x} \mathbf{Z}^T = \mathbf{C} \mathbf{Z}^T = \mathbf{X}$. Then, we have to verify that $\mathbf{U}_\mathbf{x}$ and $\mathbf{V}_\mathbf{x}$ are semi-orthogonal matrices. Proposition 1 and Eq. (13b) lead to $\mathbf{C}^T \mathbf{C} = \mathbf{S}_\mathbf{x}^2$ and so $\mathbf{U}_\mathbf{x}^T \mathbf{U}_\mathbf{x} = \mathbf{S}_\mathbf{x}^{-1} \mathbf{C}^T \mathbf{C} \mathbf{S}_\mathbf{x}^{-1} = \mathbf{I}_2$. Then, Proposition 1 and Eq. (13c) show that $\mathbf{V}_\mathbf{x}^T \mathbf{V}_\mathbf{x} = \mathbf{Z}^T \mathbf{Z} = \mathbf{I}_2$. $\square$

Remark 1. *For the particular case where $q_c = 0$, the SVD of $\mathbf{X}$ is not unique since $\mathbf{X}$ can also be decomposed as $\mathbf{X} = \mathbf{U}_\mathbf{x} \mathbf{Q} \mathbf{S}_\mathbf{x} \mathbf{Q}^T \mathbf{V}_\mathbf{x}^T$ where $\mathbf{Q}$ is an 2×2 orthogonal matrix.*

The previous proposition gives the structure of the "compact" SVD. From a geometrical point of view, it is also interesting to analyse the full SVD, which is given by

$$\mathbf{X} = \begin{bmatrix} \mathbf{U}_\mathbf{x} & \mathbf{u}_0 \end{bmatrix} \begin{bmatrix} \sigma_2 & 0 & 0 \\ 0 & \sigma_1 & 0 \\ 0 & 0 & 0 \end{bmatrix} \begin{bmatrix} \mathbf{V}_\mathbf{x}^T \\ \mathbf{v}_0^T \end{bmatrix}, \qquad (14)$$

where $\mathbf{u}_0$ and $\mathbf{v}_0$ are the left and right singular vectors associated with the null singular value of $\mathbf{X}$. Regarding the left singular vector, $\mathbf{u}_0$ can be obtained from the solution of the equation $\mathbf{C}^T \mathbf{u}_0 = \mathbf{0}$ under the unit-norm constraint $\mathbf{u}_0^T \mathbf{u}_0 = 1$. By imposing the unit-norm constraint, $\mathbf{u}_0$ can be decomposed as $\mathbf{u}_0 = \mathbf{g}/\|\mathbf{g}\|$ where $\mathbf{g}$ is the vector cross-product between the two columns of $\mathbf{C}$, i.e. $\mathbf{g} = \Re e(\mathbf{c}) \wedge \Im m(\mathbf{c}^*)$. Therefore, we obtain the following proposition[2].

---

[2]Note that this proposition constitutes a generalization of a previous result obtained in [36] for purely stationary three-phase signals.

Proposition 3. *The normal vector perpendicular to the signal subspace is given by*

$$\mathbf{u}_0 = \frac{\mathbf{g}}{\|\mathbf{g}\|}, \qquad (15)$$

where $\mathbf{g} = \Im m \left(\begin{bmatrix} c_1 c_2^* & c_2 c_0^* & c_0 c_1^* \end{bmatrix} \right)^T$.

B. Nominal condition

Under nominal condition, the three-phase signal is balanced and the corresponding complex phasors can be expressed as

$$c_k = c_0 e^{-2kj\pi/3}. \qquad (16)$$

It follows that $q_c = 0$ and $\epsilon_c = 3|c_0|^2$ and we obtain the following decomposition.

Proposition 4. *Under nominal condition, the SVD of $\mathbf{X}$ can be expressed as $\mathbf{X} = \mathbf{U}_\mathbf{x} \mathbf{S}_\mathbf{x} \mathbf{V}_\mathbf{x}^T$ where $\mathbf{U}_\mathbf{x} = \alpha \mathbf{C}$, $\mathbf{S}_\mathbf{x} = \frac{1}{\alpha} \mathbf{I}_2$, $\mathbf{V}_\mathbf{x} = \mathbf{Z}$, and $\alpha = \sqrt{\frac{2}{3|c_0|^2}}$.*

Regarding $\mathbf{u}_0$, it can be checked that $c_1 c_2^* = c_2 c_0^* = c_0 c_1^* = |c_0|^2 e^{2j\pi/3}$. Therefore, we obtain the following result.

Proposition 5. *Under nominal condition, the normal vector perpendicular to the signal subspace i.e.*

$$\mathbf{u}_0 = \mathbf{n} = \frac{1}{\sqrt{3}} \begin{bmatrix} 1 & 1 & 1 \end{bmatrix}^T. \qquad (17)$$

C. Geometrical interpretations

Several studies have shown the advantage of plotting the three-phase signal in the 3D Euclidean space [36]. As an example, Figure 1 presents the 3D trajectory for the case of an off-nominal modulated three-phase signal. The quantities defined through the SVD of Eq. (12) may be interpreted with a geometric point of view, and shed some highlights on the 3D trajectory of $\mathbf{X}$.

- From Eq. (5) and (13c), it is clear that the right singular vectors $\mathbf{V}_\mathbf{x}$ contain the real and imaginary parts of the analytic signal $z[n]$, which correlation matrix is the identity matrix (see Eq. (11a)). This indicates that the real and imaginary parts of $z[n]$ are uncorrelated and have the same energy, or equivalently that the scatter plot of $z[n]$ in the complex plane has a global circular shape.
- The diagonal matrix $\mathbf{S}_\mathbf{x}$ containing the two singular values of $\mathbf{X}$ can be interpreted as a scaling matrix applied to the previous complex-valued signal, where σ_2 is the scaling factor applied to $\Re e(z[n])$ and σ_1 is applied to $\Im m(z[n])$. Consequently, these two positive factors contain the information on the global ellipticity of the trajectory followed by $\mathbf{X}$, σ_2 being related to its semi-major axis and σ_1 to its semi-minor axis.
- The left singular vectors $\mathbf{U}_\mathbf{x}$ form an orthonormal basis for the three-phase signal $\mathbf{X}$, and therefore give the orientation of the plane containing the trajectory of the whole three-phase signal, as well as the orientation of its minor and major axes. Equivalently, the 3×3 matrix $\begin{bmatrix} \mathbf{U}_\mathbf{x} & \mathbf{u}_0 \end{bmatrix}$ appearing in the full SVD of $\mathbf{X}$ in Eq. (14) is an orthogonal matrix, and can also be interpreted as a 3D rotation matrix applied to the previous plane elliptic trajectory.
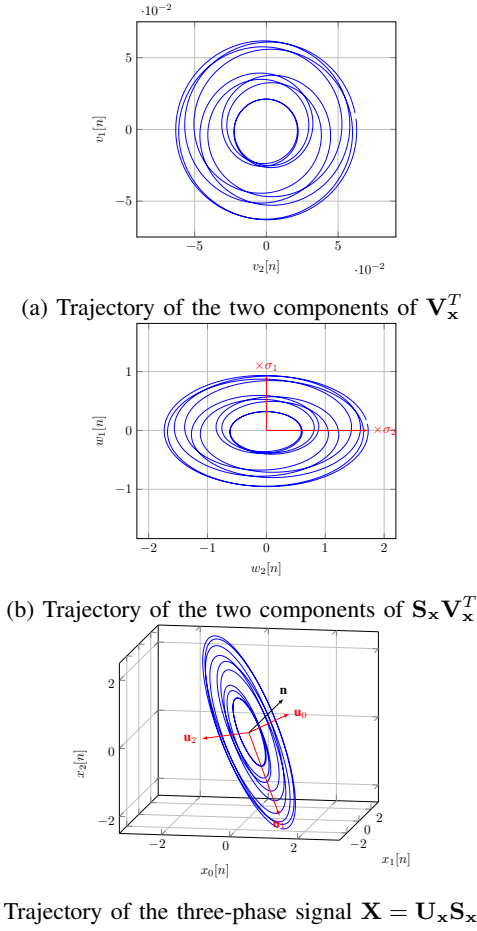
(a) Trajectory of the two components of $\mathbf{V}_\mathbf{x}^T$

(b) Trajectory of the two components of $\mathbf{S}_\mathbf{x}\mathbf{V}_\mathbf{x}^T$

(c) Trajectory of the three-phase signal $\mathbf{X} = \mathbf{U}_\mathbf{x}\mathbf{S}_\mathbf{x}\mathbf{V}_\mathbf{x}^T$

Fig. 1: Geometrical analysis of the trajectory of the three-phase signal ($c_0 = 1$, $c_1 = 0.8e^{-2.2j\pi/3}$ and $c_2 = 1.9e^{-3.9j\pi/3}$, amplitude-modulated sine wave signals).

IV. ESTIMATION / DETECTION OF OFF-NOMINAL CONDITIONS UNDER GAUSSIAN NOISE

In practice, the signal is usually corrupted by an additive noise i.e. $y_k[n] = x_k[n] + w_k[n]$. Using a matrix form, the noisy signal can be expressed as

$$\mathbf{Y} \triangleq \begin{bmatrix} y_0[0] & \cdots & y_0[N-1] \\ y_1[0] & \cdots & y_1[N-1] \\ y_2[0] & \cdots & y_2[N-1] \end{bmatrix} = \mathbf{X} + \mathbf{W}, \quad (18)$$

where $\mathbf{X} = \mathbf{C}\mathbf{Z}^T$ is the noiseless signal defined in Eq. (3) and $\mathbf{W}$ contains the additive noise. In the following, we assume that the element of $\mathbf{W}$ located in the uth row and v^{th} column, denoted $w[u,v]$, has a Gaussian distribution with zero-mean and variance equal to σ^2, i.e. $w[u,v] \sim \mathcal{N}(0,\sigma^2)$ [3]. Moreover, this noise is assumed to be white in the time domain (regarding v) and uncorrelated from phase to phase (regarding u). Note that because of the additive noise, the SVD of $\mathbf{Y}$ is generally different from that of $\mathbf{X}$. The SVD of $\mathbf{Y}$ can be expressed as

$$\mathbf{Y} = \widehat{\mathbf{U}}\widehat{\mathbf{S}}\widehat{\mathbf{V}}^T, \quad (19)$$

- $\widehat{\mathbf{U}} = [\widehat{\mathbf{u}}_2, \widehat{\mathbf{u}}_1, \widehat{\mathbf{u}}_0]$ is a 3×3 orthogonal matrix,

- $\widehat{\mathbf{S}} = \mathrm{diag}(\widehat{\sigma}_2, \widehat{\sigma}_1, \widehat{\sigma}_0)$ is a 3×3 diagonal matrix with $\widehat{\sigma}_2 \geq \widehat{\sigma}_1 \geq \widehat{\sigma}_0 \geq 0$,
- $\widehat{\mathbf{V}} = [\widehat{\mathbf{v}}_2, \widehat{\mathbf{v}}_1, \widehat{\mathbf{v}}_0]$ is a $N \times 3$ semi-orthogonal matrix.

In this section, we propose to detect unbalance systems from the structure of $\widehat{\mathbf{U}}$ and $\widehat{\mathbf{S}}$, and to estimate the angular fundamental frequency from the right singular vectors $\widehat{\widetilde{\mathbf{V}}}$.

A. Off-nominal subspace detection test

As stated in Prop. 5, the noiseless three-phase signal belongs to a plane with normal vector $\mathbf{u}_0 = \mathbf{n}$ under nominal condition. To detect a off-nominal signal subspace, we therefore propose to address the following hypothesis testing problem:

- $\mathcal{H}_0$: $\mathbf{u}_0 = \mathbf{n}$
- $\mathcal{H}_1$: $\mathbf{u}_0 \neq \mathbf{n}$;

where $\mathbf{n}$ is defined in (17). Then, we propose to use a GLRT detector for choosing between the two hypothesis. This detector chooses $\mathcal{H}_1$ if

$$\mathcal{T}_\mathbf{n}(\mathbf{Y}, \sigma^2) = 2\ln\left(\frac{\mathcal{L}(\mathbf{Y}; \widehat{\mathbf{Z}}, \sigma^2, \mathcal{H}_1)}{\mathcal{L}(\mathbf{Y}; \widehat{\mathbf{Z}}, \sigma^2, \mathcal{H}_0)}\right) > \tau, \quad (20)$$

where $\mathcal{L}(\mathbf{Y}; \mathbf{Z}, \sigma^2, \mathcal{H}_k)$ corresponds to the likelihood function of $\mathbf{Y}$ [37, Section 6.5]. It is demonstrated in appendix A that

$$\mathcal{T}_\mathbf{n}(\mathbf{Y}, \sigma^2) = \frac{1}{\sigma^2}(\|\mathbf{n}^T\mathbf{Y}\|_F^2 - \widehat{\sigma}_0^2). \quad (21)$$

This detector relies on the difference between two positive terms normalized by the noise variance. Obviously, $\mathcal{T}_\mathbf{n}(\mathbf{Y}, \sigma^2)$ is close to zero under nominal condition, and positive otherwise. Moreover, under assumption $\mathcal{H}_0$, it is known that the GLRT follows a chi-squared distribution with r degrees of freedom, where r corresponds to the number of free parameters under $\mathcal{H}_0$ [37, Section 6.5]. As $\mathbf{u}_0$ is a 3 unit-norm column vector, it follows that the criterion follows under $\mathcal{H}_0$ a chi-squared distribution with 2 degrees of freedom, i.e. $\mathcal{T}_\mathbf{n}(\mathbf{Y}, \sigma^2) \sim \chi_2^2$. Note that the evaluation of $\mathcal{T}_\mathbf{n}(\mathbf{Y}, \sigma^2)$ requires the knowledge of the noise variance. When the noise variance is unknown, we propose to replace it by the following estimator $\widehat{\sigma}^2 = \frac{\widehat{\sigma}_0^2}{N}$. For large N, as the variance of $\widehat{\sigma}^2$ is negligible as compared to the variance of $\mathcal{T}_\mathbf{n}(\mathbf{Y}, \sigma^2)$, the distribution of $\mathcal{T}_\mathbf{n}(\mathbf{Y}, \widehat{\sigma}^2)$ can be approximated by the distribution of $\mathcal{T}_\mathbf{n}(\mathbf{Y}, \sigma^2)$. Using this approximation, we obtain the following proposition.

Proposition 6. *The GLRT detector chooses hypothesis $\mathcal{H}_1$ if*

$$\mathcal{T}_\mathbf{n}(\mathbf{Y}) = \frac{N}{\widehat{\sigma}_0^2}(\|\mathbf{n}^T\mathbf{Y}\|_F^2 - \widehat{\sigma}_0^2) = N\left(\frac{\|\mathbf{n}^T\mathbf{Y}\|_F^2}{\widehat{\sigma}_0^2} - 1\right) \quad (22)$$

is greater than a threshold τ_m. Furthermore, under $\mathcal{H}_0$, $\mathcal{T}_\mathbf{n}(\mathbf{Y})$ follows, asymptotically, a chi-squared distribution with 2 degrees of freedom.

In practice, the test threshold τ_m can be set according to the desired probability of false alarm, $p_{fa} \triangleq 1 - \int_0^{\tau_m} p(\mathcal{T}_\mathbf{n}(\mathbf{Y}) = x|\mathcal{H}_0)dx$. Indeed, by using Proposition 6, we obtain

$$p(\mathcal{T}_\mathbf{n}(\mathbf{Y}) = x|\mathcal{H}_0) = \begin{cases} \frac{1}{2}e^{-\frac{1}{2}x} & x > 0 \\ 0 & x < 0 \end{cases} \quad (23)$$

and so $\tau_m = -2\ln(p_{fa})$.

B. Ellipticity detection test

Under nominal conditions the two largest singular values of the three-phase signal are equal. Then, we propose to address the following ellipticity detection test:

- $\mathcal{H}_0$: the signal is globally circular i.e. $\sigma_2 = \sigma_1$,
- $\mathcal{H}_1$: the signal is not globally circular i.e. $\sigma_2 \neq \sigma_1$,

The GLRT detector chooses $\mathcal{H}_1$ if

$$\mathcal{T}_\sigma(\mathbf{Y}, \sigma^2) = 2\ln\left(\frac{\mathcal{L}(\mathbf{Y}; \widehat{\mathbf{X}}, \sigma^2, \mathcal{H}_1)}{\mathcal{L}(\mathbf{Y}; \widehat{\mathbf{X}}, \sigma^2, \mathcal{H}_0)}\right) > \tau. \quad (24)$$

It is demonstrated in the Appendix B that

$$\mathcal{T}_\sigma(\mathbf{Y}, \sigma^2) = \frac{1}{2\sigma^2}(\widehat{\sigma}_2 - \widehat{\sigma}_1)^2. \quad (25)$$

This equation shows that the GLRT approach leads to a simple intuitive criterion that is equal to the weighted squared difference of the two largest singular values. This criterion can also be viewed as the weighted squared difference between the semi-major and semi-minor axes of the ellipse approximating the signal 3D trajectory. Under assumption $\mathcal{H}_0$, the two singular values are nearly equal and their difference is close to 0 i.e. $\mathcal{T}_\sigma(\mathbf{Y}, \sigma^2) \approx 0$. Under assumption $\mathcal{H}_0$ and additive Gaussian noise, thank's to the properties of the GLRT, the decision statistic follows asymptotically a chi-squared distribution with 2 degrees of freedom, i.e. $\mathcal{T}_\sigma(\mathbf{Y}, \sigma^2) \sim \chi_2^2$. When the noise variance is unknown, we propose to replace σ^2 by $\widehat{\sigma}^2 = \frac{\widehat{\sigma}_0^2}{N}$ using similar arguments as in section IV-A.

Proposition 7. *The GLRT detector chooses hypothesis $\mathcal{H}_1$ if*

$$\mathcal{T}_\sigma(\mathbf{Y}) = \frac{N}{2\widehat{\sigma}_0^2}(\widehat{\sigma}_2 - \widehat{\sigma}_1)^2 \quad (26)$$

is greater than a threshold τ_m. Furthermore, under hypothesis $\mathcal{H}_0$, $\mathcal{T}_\sigma(\mathbf{Y})$ follows, asymptotically, a chi-squared distribution with 2 degrees of freedom.

C. Estimation of the angular frequency

The analytic signal $\mathbf{z}$ can be estimated from the 2 principal right-singular vectors $\widehat{\mathbf{V}}_\mathbf{x} = [\widehat{\mathbf{v}}_2, \widehat{\mathbf{v}}_1]$ as $\widehat{\mathbf{z}} = \widehat{\mathbf{v}}_2 + j\widehat{\mathbf{v}}_1$. It is demonstrated in Appendix C that the estimated analytic signal $\widehat{\mathbf{z}} = [\widehat{z}[0], \cdots, \widehat{z}[N-1]]^T$ can be approximated by

$$\widehat{z}[n] \approx a[n]e^{j(\rho\phi[n]+\varphi)} + b[n], \quad (27)$$

where $b[n]$ contains the additive noise, φ corresponds to an unknown phase-shift and $\rho \in \{1, -1\}$. Regarding the additive noise, as $w[u, v] \sim \mathcal{N}(0, \sigma^2)$, $b[n]$ follows a complex zero-mean noncircular white Gaussian distribution. Note that the additive noise becomes circular if and only if $\widehat{\sigma}_1^2 = \widehat{\sigma}_2^2$. In the following, we show how to accurately estimate the signal angular frequency from $\widehat{z}[n]$ for the particular case where the instantaneous amplitude is constant, i.e. $z[n] = ce^{j\omega_0 n}$. To estimate the unknown signal parameters, a natural approach is to minimize the sum of squared residuals between $\widehat{z}[n]$ and $ce^{j\omega_0 n}$. Mathematically, the Least-Squares (LS) estimator is then given by

$$\{\widehat{\rho}, \widehat{\omega}_0, \widehat{c}\} = \arg\min_{r,\omega,c} \sum_{n=0}^{N-1} |\widehat{z}[n] - ce^{jr\omega n}|^2, \quad (28)$$

where $r \in \{1, -1\}$, $\omega \in [0, \pi[$ and $c \in \mathbb{C}$. In the following, instead of minimizing the LS cost-function directly, we propose an alternative low-complexity technique based on the decoupled estimation of ρ, ω_0, and c.

1) Estimation of ρ: As $z[n]$ is an analytic signal, its Discrete Time Fourier Transform is equal to 0 for $-\pi < \omega < 0$ (modulo 2π). In order to estimate ρ, a simple solution is to compare the energy of $\widehat{z}[n]$ in the frequency band $0 < \omega < \pi$ to the one in the band $\pi < \omega < 2\pi$. Specifically, let us define the DTFT of the truncated signal $\widehat{z}$ as

$$Z_m \triangleq \sum_{n=0}^{M-1} \widehat{z}[n]e^{-j\frac{2\pi nm}{M}}, \quad (29)$$

where $M < N$ is the truncated signal length. Then, a simple estimator of ρ is given by

$$\widehat{\rho} = \begin{cases} 1 & \text{if } \sum_{m=0}^{M/2-1} |Z_m|^2 \geq \sum_{m=M/2}^{M-1} |Z_m|^2 \\ -1 & \text{elsewhere} \end{cases}. \quad (30)$$

2) Estimation of c and ω_0: In (28), it can be checked that the LS cost-function is minimized when $c = \frac{1}{N}\sum_{n=0}^{N-1} \widehat{z}[n]e^{-jr\omega n}$ [38]. Then, by replacing c and ρ by their estimate, the angular frequency estimator can be obtained from the maximizer of the direction-corrected Periodogram of $\widehat{\mathbf{z}}$ i.e.

$$\widehat{\omega}_0 = \arg\max_\omega \frac{1}{N}\left|\sum_{n=0}^{N-1} \widehat{z}[n]e^{-j\widehat{\rho}\omega n}\right|^2. \quad (31)$$

D. Algorithms Summary

Under additive Gaussian noise, we have proposed two techniques for the detection of unbalanced systems: the first one is described by the Algorithm 1 and can be used to detect an off-nominal signal subspace, the second one is described by the Algorithm 2 and can be used to detect an elliptic signal trajectory. The proposed frequency estimator is described by the Algorithm 3. Figure 2 shows how to combine these algorithms for the analysis of three-phase signals. From a physical viewpoint, it should be mentioned that the proposed detectors can distinguish between two classes of unbalanced systems. Specifically, the first class corresponds to the case where the zero-sequence is not equal to 0 while the second one corresponds to the case where the signal is not circular in the 2D plane. If a three-phase signal belongs, at least, to one of these classes, then the system is unbalanced. Note that these two classes are not exclusive since some unbalanced systems may have a non-null zero-sequence component and be non-circular in the 2D plane.

V. SIMULATION RESULTS

To highlight the interest of this study, this section reports on the performance of the proposed techniques with Monte Carlo simulations. In each simulation, the three-phase signal is described by the signal model in (18) where $w[u, v] \sim \mathcal{N}(0, \sigma^2)$. Concerning the analytic signal, $z[n] = ce^{j\omega_0 n}$ where the (normalized) angular frequency is given by $\omega_0 = 2\pi f_0/F_s = 120\pi/F_s$, $f_0 = 60$ Hz corresponds to the signal frequency, and
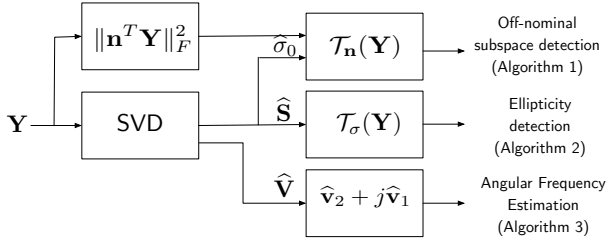
Fig. 2: Analysis of three-phase signals using SVD

Algorithm 1 Blind Off-nominal subspace detection test

Input: Three Phase Signal $\mathbf{Y}$, threshold τ_m.
Output: detected (True or False)
 1: Compute the SVD of $\mathbf{Y} = \widehat{\mathbf{U}}\widehat{\mathbf{S}}\widehat{\mathbf{V}}^T$
 2: Extract the smallest singular value $\widehat{\sigma}_0$ from $\widehat{\mathbf{S}}$
 3: Compute $\|\mathbf{n}^T\mathbf{Y}\|_F^2$
 4: Compute the test criterion $\mathcal{T}_\mathbf{n}(\mathbf{Y})$ in (22).
 5: **if** $(\mathcal{T}_\mathbf{n}(\mathbf{Y}) > \tau_m)$ **then**
 6:     detected $\leftarrow$ True
 7: **else**
 8:     detected $\leftarrow$ False
 9: **end if**
10: **return** detected

Algorithm 2 Blind Ellipticity detection test

Input: Three Phase Signal $\mathbf{Y}$, threshold τ_σ.
Output: detected (True or False)
 1: Compute the SVD of $\mathbf{Y} = \widehat{\mathbf{U}}\widehat{\mathbf{S}}\widehat{\mathbf{V}}^T$
 2: Extract the three singular values $\widehat{\sigma}_2 \geq \widehat{\sigma}_1 \geq \widehat{\sigma}_0$ from $\widehat{\mathbf{S}}$
 3: Compute the test criterion $\mathcal{T}_\sigma(\mathbf{Y})$ in (26).
 4: **if** $(\mathcal{T}_\sigma(\mathbf{Y}) > \tau_\sigma)$ **then**
 5:     detected $\leftarrow$ True
 6: **else**
 7:     detected $\leftarrow$ False
 8: **end if**
 9: **return** detected

Algorithm 3 Angular frequency Estimator

Input: Three Phase Signal $\mathbf{Y}$, truncated signal length M
Output: Angular frequency ω_0
 1: Compute the SVD of $\mathbf{Y} = \widehat{\mathbf{U}}\widehat{\mathbf{S}}\widehat{\mathbf{V}}^T$
 2: Estimate the analytical signal with $\widehat{\mathbf{z}} = \widehat{\mathbf{v}}_2 + j\widehat{\mathbf{v}}_1$
 3: Compute the DTFT of the truncated signal $z[n]$ ($n = 0, \cdots, M-1$).
 4: Estimate the rotating direction ρ using (30).
 5: Estimate ω_0 by maximizing the direction-corrected periodogram of $\widehat{\mathbf{z}}$ in (31) using an optimisation algorithm.
 6: **return** $\widehat{\omega}_0$

$F_s = 60 \times 24 = 1440$ Hz is the sampling rate. Using these parameters, the cycle duration is equal to $N = 24$ samples. For the considered signal, it should be mentioned that the requirement in (10) is only satisfied when $N = k\pi/\omega_0 = 12k$ ($k \in \mathbb{N}$) or asymptotically when $N \gg \frac{\pi}{\omega_0}$. The values of c_k are set according to one of the configurations in Table I, where the four configurations refer respectively to a perfectly balanced

TABLE I: Phasor Configuration

Phasor	c_0	c_1	c_2
Configuration 1	1	$e^{-j2\pi/3}$	$e^{-j4\pi/3}$
Configuration 2	1	$0.9 \times e^{-j2\pi/3}$	$0.95 \times e^{-j4\pi/3}$
Configuration 3	1	$0.95 \times e^{-j2\pi/3}$	$0.95 \times e^{-j4\pi/3}$
Configuration 4	1	$0.8 \times e^{-j2\pi/3}$	$0.3 \times e^{-j4\pi/3}$

signal ($\mathbf{u}_0 = \mathbf{n}$ and $\sigma_2 = \sigma_1$), a signal with off-nominal subspace ($\mathbf{u}_0 \neq \mathbf{n}$), a non-circular signal ($\sigma_2 \neq \sigma_1$), and a full unbalanced signal. In the following simulations, the Signal to Noise Ratio (SNR) is defined as $SNR = 10\log(\|\mathbf{c}\|^2/(6\sigma^2))$ and the performance is estimated from 10^4 Monte Carlo trials.
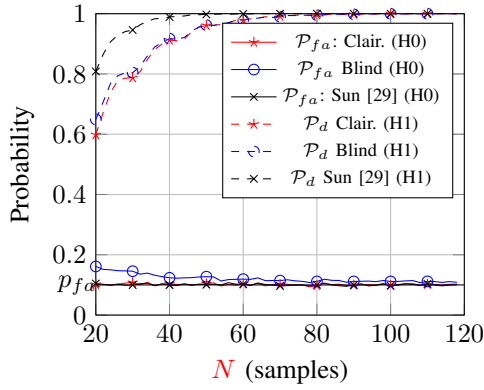
A. Off-nominal subspace detection

This subsection presents the performance of several detectors for the discrimination of phasor configurations 1 and 2 in Table I. In each simulation, three detectors are considered: the clairvoyant detector that requires a perfect knowledge of σ^2 (denoted *clair.*), the blind detector (denoted *blind*), and the GLRT detector proposed by *Sun* that requires a perfect knowledge of σ^2 and ω_0 [29]. Mathematically, the clairvoyant and blind detectors are based on the GLRT expressions given by Eqs.(21) and (22), respectively.

Figure 3a gives the probabilities of detection, $\mathcal{P}_d$, and false alarm, $\mathcal{P}_{fa}$, versus the signal length N when the test threshold is computed as $\tau_m = -2\ln(p_{fa})$ with $p_{fa} = 0.1$. We observe that the three detectors allow to detect the off-nominal subspaces with high probability when $N > 80$ samples. In particular, the proposed blind and clairvoyant detectors perform well even if the condition $q_z = 0$ is not perfectly fulfilled. Moreover, we note that the experimental probability of false alarm is close to its theoretical value, $p_{fa} = 0.1$, from $N = 100$ samples. Figure 3b shows the Receiver Operating Characteristic (ROC) curve i.e. the probability of detection versus the probability of false alarm for different values of the test threshold τ_m. The ROC curves are evaluated for $N = 48$ samples and different SNRs. We observe that the clairvoyant and blind detectors have similar performance whatever the SNR. We also note that the *Sun* detector clearly outperforms the two proposed detectors whatever the SNR. Nevertheless, it should be mentioned that the performance of the *Sun* detector, which has been designed for perfectly sine-wave signals, significantly degrades in the presence of dynamic conditions. To illustrate this behavior, Fig 3c presents the evolution of the experimental probability of false alarm in presence of amplitude modulation. We see that *Sun* detector is not able to maintain the probability of false alarm to $p_{fa} = 0.1$ when the modulation index increases, while the two proposed detectors are insensitive to the presence of amplitude modulation.

B. Ellipticity detection

This subsection reports on the performance of several detectors for the discrimination of phasor configurations 1 and 3 in Table I. In each simulation, three detectors are considered: the proposed clairvoyant detector, the proposed blind detector, and the *Sun* detector [29]. The two proposed detectors are based on the equations (25) and (26), respectively. Figure 4a
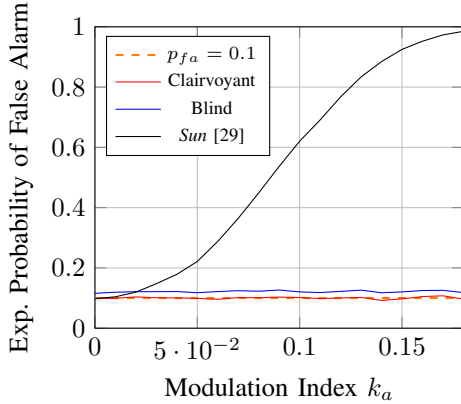
(a) Probabilities of detection ($\mathcal{P}_d$) and false alarm ($\mathcal{P}_{fa}$) versus N ($SNR = 20$ dB, $p_{fa} = 0.1$).
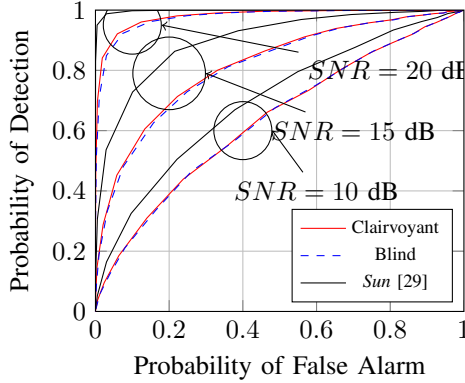
(b) ROC curves ($N = 48$ samples, 2 cycles).

(c) Experimental Probability of False Alarm versus Modulation index ($SNR = 40$ dB, $N = 48$ samples, $p_{fa} = 0.1$, $a[n] = 1 + k_a \cos(2\pi(5/F_s)n)$).

Fig. 3: Off-nominal subspace detection (phasor configurations 1 and 2 in Table I, $\omega_0 = 120\pi/F_s$)

shows the values of $\mathcal{P}_d$ and $\mathcal{P}_{fa}$ versus the signal length N when $p_{fa} = 0.1$. We observe that the probabilities of detection and false alarm exhibit strong oscillations for the two proposed detectors. These oscillations are caused by the fact that the assumption $q_z = 0$ is not fulfilled for small values of N. We also note that the experimental probability of false alarm seems to be exactly equal to its expected value when $N = 12k$ ($k \in \mathbb{N}$). Figure 4b presents the Receiver Operating Characteristic (ROC) for the two detectors when

$N = 48$ samples. We observe that a large SNR is required to guarantee satisfying performance. Figure 4c reports on the ability for the three detectors to maintain the probability of false alarm in presence of amplitude modulation. We see that the performance of the considered techniques critically depend on the number of samples. Indeed, we observe that the three detectors are not able to maintain the probability of false alarm when $N = 48$ samples, but lead to satisfactory results when $N = 288$ samples. As compared to the proposed techniques, we observe that the *Sun* detector clearly outperforms the proposed approaches for ellipticity detection. Nevertheless, it should be emphasized that this detector requires a perfect knowledge of the fundamental frequency and noise variance, while our techniques can be used without a priori information about these parameters.

C. Angular frequency estimation

In this section, we focus on the angular frequency estimation problem. Specifically, this section compares the performance of the following techniques for frequency estimation.

- The proposed SVD-based estimator described in subsection IV-C (SVD).
- The DTFT algorithm obtained by maximizing the periodogram of the signal on the first phase $x_0[n]$ [13].
- The Maximum Likelihood Estimator (ML) [10].
- The Maximum Likelihood Estimator under balanced assumption (ML-bal) [25],
- The Clarke-based approximate Maximum Likelihood Estimator (ML-Clarke) [7],

For these techniques, the frequency estimate is obtained by maximizing a cost-function whose evaluation requires the computation of several DTFTs. These cost-functions are maximized by using the Nelder-Mead optimisation algorithm with an initial value $\omega_{init} = 120\pi/F_s$ [39]. For the proposed estimator, the SVD has been implemented using the `svd()` subroutine of Python/Numpy and the rotating direction has been estimated from (30) with $M = 8$. To assess the estimator performances, the Mean Square Error $MSE \triangleq E[(\omega_0 - \widehat{\omega}_0)^2]$ has been evaluated using several Monte Carlo trials. Note that the MSE can be decomposed as $MSE(\widehat{\omega}_0) = \text{var}(\widehat{\omega}_0) + \text{bias}^2(\omega_0, \widehat{\omega}_0)$ where $\text{var}(\widehat{\omega}_0)$ is the estimator variance and $\text{bias}(\omega_0, \widehat{\omega}_0) = E(\widehat{\omega}_0) - \omega_0$ corresponds to the estimator bias [38]. In each trial, the angular frequency is set to $\omega_0 = 2\pi \times 65/F_s$ ($f_0 = 65$Hz) and the phasors are given by the configuration 4 in Table I. The approximate Cramér-Rao Bound $CRB = \frac{24\sigma^2}{N^3 \|c\|^2}$ is also reported for comparison [10].

Figure 5a presents the evolution of the MSE versus N. We observe that the ML estimator achieves optimal performance for $N > 20$ samples. Concerning the ML-Clarke and ML-bal techniques, we note that the MSE exhibits a strong oscillation with period $N \approx 12$ samples. To explain this behavior, Fig. 5b reports on the estimator bias for the considered techniques. We see that the oscillations of the MSE for the DTFT, ML-Clarke and ML-bal techniques are due to the estimator bias. We also note that the contribution of the bias seems to be negligible for the proposed and ML techniques. Finally, Figure 5c shows the influence of the SNR on the MSE. Except for the ML
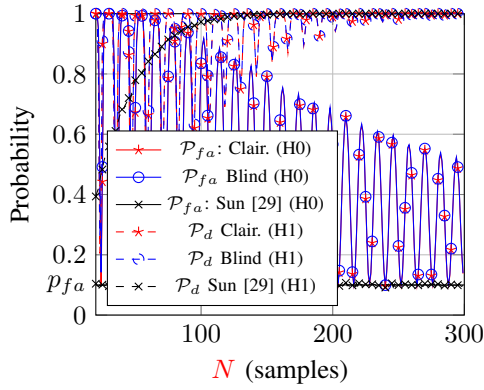
(a) Probabilities of detection ($\mathcal{P}_d$) and false alarm ($\mathcal{P}_{fa}$) versus N ($SNR = 20$ dB, $p_{fa} = 0.1$).
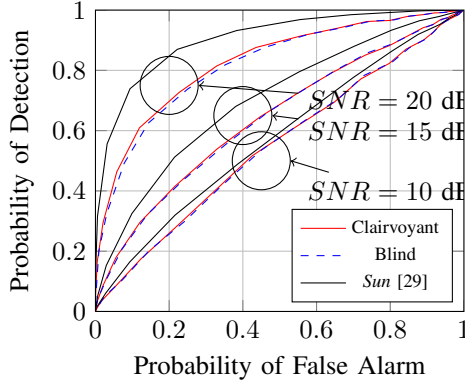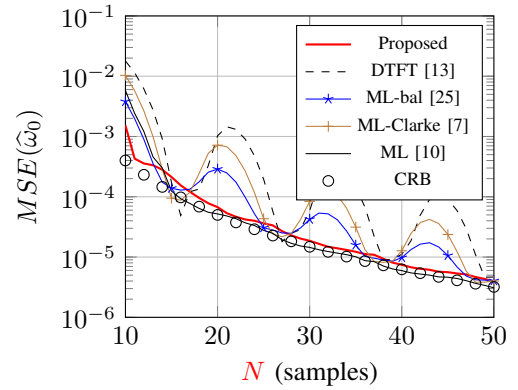

(b) ROC curves ($N = 48$ samples, 2 cycles).
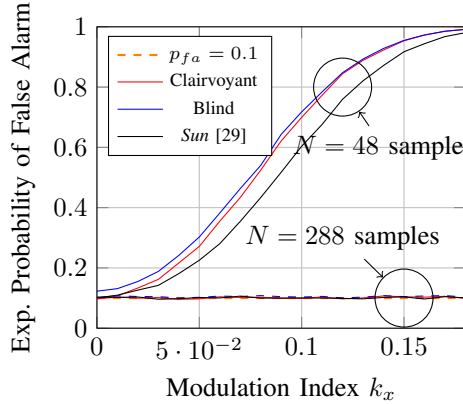
(c) Experimental Probability of False Alarm versus Modulation index k_x ($SNR = 40$ dB, $p_{fa} = 0.1$, $a[n] = 1 + k_a \cos(2\pi(5/F_s)n)$).
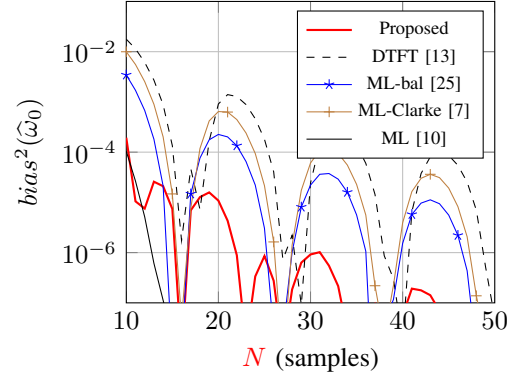
Fig. 4: Ellipticity detection (phasor configurations 1 and 3 in Table I, $\omega_0 = 120\pi/F_s$)

(a) Angular frequency estimation: Mean Squared Error ($SNR = 10$ dB)

(b) Angular frequency estimation: Estimator bias^2 ($SNR = 10$ dB)

(c) Angular frequency estimation: Mean Squared Error ($N = 24$ samples)

Fig. 5: Angular Frequency Estimation (phasor configuration 4 in Table I, $\omega_0 = 2\pi \times 65/F_s$).

technique, we observe that the estimators exhibit an error floor at SNR > 30 dB. This error floor appears to be caused by the estimator bias for finite N.
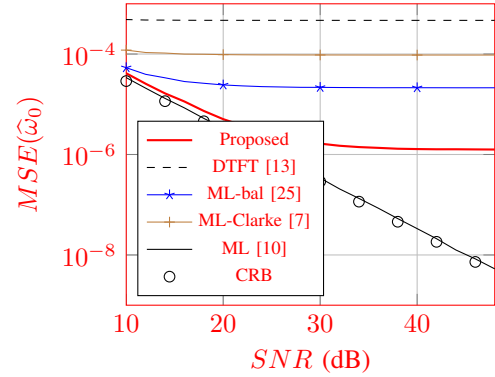
To evaluate the estimator performance, the IEEE Standard C37.118.1-2011 has introduced a criterion called the Frequency Error (FE) which is defined as $FE = |f_0 - \widehat{f}_0|$ [40]. To be compliant with this standard, the frequency error must be bounded by $FE < 0.005$. As pointed out in [10], when the signal is corrupted by an additive noise, this criterion is not well suited for the analysis of the estimation performance since the frequency error becomes a random variable. In this context, a natural extension is to evaluate the probability of Frequency Error compliance, i.e. $P_{FE} \triangleq P[|f_0 - \widehat{f}_0| < 0.005]$. Figure 6 presents the evolution of P_{FE} versus N. It shows that the performance of the proposed estimator is closed to the one of the ML technique, and that the performance of the other estimators are strongly affected by the presence of the estimator bias.
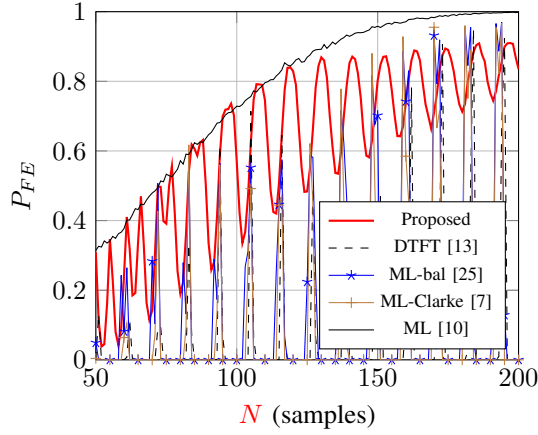
Fig. 6: Probability of FE Compliance ($SNR = 40$ dB)

TABLE II: Average Computation time per trial versus N

Technique	$N = 50$	$N = 100$	$N = 150$
Proposed	0.71ms	0.83ms	1.05ms
DTFT [13]	0.58ms	0.67ms	0.83 ms
ML-bal [25]	0.58ms	0.70ms	0.88 ms
ML-Clarke [7]	0.80ms	1.02ms	1.33 ms
ML [10]	1.72ms	2.00ms	2.40ms

Table II reports on the average computational time for the considered estimators. These estimators have been implemented using Python and the simulations have been run on an Linux machine with an Intel CoreTM i7-6700 processor (CPU at 3.4 Ghz). We observe that the proposed technique has a lower computational complexity than the recently proposed ML-Clarke technique. This result is not surprising since the ML-Clarke cost-function is composed of 2 DTFTs while the proposed cost-function only requires the computation of 1 DTFT.

VI. CONCLUSION

In this paper, we have proposed a new approach for the analysis of three-phase signals based on the SVD. Instead of using a fixed transform for signal analysis, the SVD directly exploits the content of the three-phase signal for dimensional reduction and gives a better insight into the signal structure. Under additive white Gaussian noise, we have developed two Generalized Likelihood Ratio Tests for the detection of off-nominal condition based on the SVD: the off-nominal subspace detector aiming at detecting $\mathbf{u}_0 \neq \mathbf{n}$, and the eccentricity detector aiming at detecting $\sigma_2 \neq \sigma_1$. Furthermore, we have derived a new low-complexity angular frequency estimator based on the Periodogram of the right-singular vector. Simulation results have shown that the proposed detectors perform well even for a small number of samples and that the proposed angular frequency estimator gives a good compromise between statistical performance and computational complexity.

APPENDIX A
DERIVATION OF $\mathcal{T}_\mathbf{n}(\mathbf{Y}, \sigma^2)$

As $w[u, v] \sim \mathcal{N}(0, \sigma^2)$, we obtain

$$\mathcal{L}(\mathbf{Y}; \mathbf{Z}, \sigma^2, \mathcal{H}_k) = \beta e^{-\frac{1}{2\sigma^2}\|\mathbf{Y} - \mathbf{C}\mathbf{Z}^T\|_F^2} \qquad (32)$$

where $\|.\|_F^2$ corresponds to the Frobenius norm and $\beta = \left(\frac{1}{2\pi\sigma^2}\right)^{\frac{3N}{2}}$. In practice, the matrix $\mathbf{Z}^T$ is unknown and can be replaced by its Maximum Likelihood estimate $\widehat{\mathbf{Z}}^T = \left(\mathbf{C}^T\mathbf{C}\right)^{-1}\mathbf{C}^T\mathbf{Y}$ [38, Chapter 7]. Let us introduce $\mathbf{P}_\mathbf{C}^\perp \triangleq \mathbf{I} - \mathbf{C}(\mathbf{C}^T\mathbf{C})^{-1}\mathbf{C}^T$, the orthogonal projector into the null space of $\mathbf{C}$. As $\mathbf{C}$ is a 3×2 matrix, this projector can be decomposed as $\mathbf{P}_\mathbf{C}^\perp = \mathbf{u}_0\mathbf{u}_0^T$ [14, Result R17]. Therefore,

$$\mathcal{L}(\mathbf{Y}; \widehat{\mathbf{Z}}, \sigma^2, \mathcal{H}_k) = \beta e^{-\frac{1}{2\sigma^2}\|\mathbf{P}_\mathbf{C}^\perp\mathbf{Y}\|_F^2} = \beta e^{-\frac{1}{2\sigma^2}\|\mathbf{u}_0^T\mathbf{Y}\|_F^2}$$

where $\mathbf{u}_0 = \mathbf{n}$ under assumption $\mathcal{H}_0$. Under assumption $\mathcal{H}_1$, $\mathbf{u}_0$ is given by $\widehat{\mathbf{u}}_0$ [41, Section 4.2]. As $\|\widehat{\mathbf{u}}_0^T\mathbf{Y}\|_F^2 = \widehat{\sigma}_0^2$, Eq. (20) can be simplified as in Eq. (21).

APPENDIX B
DERIVATION OF $\mathcal{T}_\sigma(\mathbf{Y}, \sigma^2)$

As $w[u, v] \sim \mathcal{N}(0, \sigma^2)$, we obtain

$$\mathcal{L}(\mathbf{Y}; \mathbf{X}, \sigma^2, \mathcal{H}_k) = \beta e^{-\frac{1}{2\sigma^2}\|\mathbf{Y} - \mathbf{X}\|_F^2}. \qquad (33)$$

To evaluate the likelihood-function, $\mathbf{X}$ must be replaced by its MLE. Two cases must be distinguished. Under $\mathcal{H}_1$, the MLE of $\mathbf{X}$ is found by minimizing the Frobenius norm $\|\mathbf{Y} - \widehat{\mathbf{X}}\|_F^2$ where $\widehat{\mathbf{X}}$ is a rank-2 matrix. The Eckart-Young theorem states that this norm is minimized for $\widehat{\mathbf{X}} = \widehat{\mathbf{U}}\widehat{\mathbf{S}}_1\widehat{\mathbf{V}}^T$ where

$$\widehat{\mathbf{S}}_1 = \begin{bmatrix} \widehat{\sigma}_2 & 0 & 0 \\ 0 & \widehat{\sigma}_1 & 0 \\ 0 & 0 & 0 \end{bmatrix}. \qquad (34)$$

Under $\mathcal{H}_0$, the MLE of $\mathbf{X}$ is found by minimizing the Frobenius norm $\|\mathbf{Y} - \widehat{\mathbf{X}}\|_F^2$, where $\widehat{\mathbf{X}}$ is a rank-2 matrix with equal singular values. Then, the estimator of $\mathbf{X}$ can be decomposed as $\mathbf{X} = \widehat{\mathbf{U}}\widehat{\mathbf{S}}_0\widehat{\mathbf{V}}^T$ where

$$\widehat{\mathbf{S}}_0 = \widehat{\sigma} \times \begin{bmatrix} 1 & 0 & 0 \\ 0 & 1 & 0 \\ 0 & 0 & 0 \end{bmatrix}. \qquad (35)$$

The singular value $\widehat{\sigma}$ is found by minimizing $\|\mathbf{Y} - \widehat{\mathbf{U}}\widehat{\mathbf{S}}_0\widehat{\mathbf{V}}^T\|_F^2 = \|\widehat{\mathbf{S}} - \widehat{\mathbf{S}}_0\|_F^2$ with respect to $\widehat{\sigma}$. After some computations, we obtain $\widehat{\sigma} = \frac{1}{2}(\widehat{\sigma}_1 + \widehat{\sigma}_2)$.

By using these two results, Eq. (33) can be expressed as

$$\mathcal{L}(\mathbf{Y}; \widehat{\mathbf{X}}, \sigma^2, \mathcal{H}_k) = \beta e^{-\frac{1}{2\sigma^2}\|\mathbf{Y} - \widehat{\mathbf{U}}\widehat{\mathbf{S}}_k\widehat{\mathbf{V}}^T\|_F^2} = \beta e^{-\frac{1}{2\sigma^2}\|\widehat{\mathbf{S}} - \widehat{\mathbf{S}}_k\|_F^2}.$$

Then, by using the fact that $\widehat{\sigma} = \frac{1}{2}(\widehat{\sigma}_1 + \widehat{\sigma}_2)$, we obtain

$$\mathcal{T}_\sigma(\mathbf{Y}, \sigma^2) = \frac{1}{\sigma^2}\left(\|\widehat{\mathbf{S}} - \widehat{\mathbf{S}}_0\|_F^2 - \|\widehat{\mathbf{S}} - \widehat{\mathbf{S}}_1\|_F^2\right) = \frac{1}{2\sigma^2}(\widehat{\sigma}_2 - \widehat{\sigma}_1)^2.$$

APPENDIX C
EXPRESSION OF $\widehat{z}[n]$

The analytic signal $\mathbf{z}$ is estimated from the 2 principal right-singular vectors $\widehat{\mathbf{V}}_\mathbf{x} = [\widehat{\mathbf{v}}_2, \widehat{\mathbf{v}}_1]$. These vectors can be computed as $\widehat{\mathbf{V}}_\mathbf{x}^T = \widehat{\mathbf{S}}_\mathbf{x}^{-1}\widehat{\mathbf{U}}_\mathbf{x}^T\mathbf{Y}$ where $\widehat{\mathbf{S}}_\mathbf{x}$ and $\widehat{\mathbf{U}}_\mathbf{x}$ correspond to the 2 largest singular values of $\mathbf{Y}$ and their associated left singular vectors.

For large N and small σ^2, $\widehat{\mathbf{C}} = \widehat{\mathbf{U}}_{\mathbf{x}}\widehat{\mathbf{S}}_{\mathbf{x}} \approx \mathbf{CQ}$ where $\mathbf{Q}$ is an orthogonal matrix containing the SVD indeterminations. By using this property, it follows that

$$\widehat{\mathbf{V}}_{\mathbf{x}}^T = \widehat{\mathbf{S}}_{\mathbf{x}}^{-1}\widehat{\mathbf{U}}_{\mathbf{x}}^T\mathbf{Y} = \widehat{\mathbf{S}}_{\mathbf{x}}^{-1}\widehat{\mathbf{U}}_{\mathbf{x}}^T\mathbf{CZ}^T + \widehat{\mathbf{S}}_{\mathbf{x}}^{-1}\widehat{\mathbf{U}}_{\mathbf{x}}^T\mathbf{W}$$
$$\approx \mathbf{Q}^T\mathbf{Z}^T + \widehat{\mathbf{S}}_{\mathbf{x}}^{-1}\widehat{\mathbf{U}}_{\mathbf{x}}^T\mathbf{W}.$$

As $\mathbf{Q}$ is an 2×2 orthogonal matrix, $\mathbf{Q} \in \{\mathbf{Q}_1, \mathbf{Q}_2\}$ where

$$\mathbf{Q}_1 \triangleq \begin{bmatrix} \cos(\theta) & -\sin(\theta) \\ \sin(\theta) & \cos(\theta) \end{bmatrix}, \quad \mathbf{Q}_2 \triangleq \begin{bmatrix} \cos(\theta) & \sin(\theta) \\ \sin(\theta) & -\cos(\theta) \end{bmatrix}.$$

Then, the estimator of the analytic signal can be obtained as

$$\widehat{\mathbf{z}} \triangleq \widehat{\mathbf{V}}_{\mathbf{x}} \begin{bmatrix} 1 \\ j \end{bmatrix} \approx \begin{cases} e^{-j\theta}\mathbf{z} + \mathbf{b} & \text{if } \mathbf{Q} = \mathbf{Q}_1 \\ e^{j\theta}\mathbf{z}^* + \mathbf{b} & \text{if } \mathbf{Q} = \mathbf{Q}_2 \end{cases}, \quad (36)$$

where $\mathbf{b}$ is an additive white complex noise. Finally, using the definition of $\mathbf{z}$, Eq. (36) can be expressed as in Eq. (27).

REFERENCES

[1] M. Bollen and I. Gu, *Signal processing of power quality disturbances*. John Wiley & Sons, 2006, vol. 30.

[2] P. Top, M. Bell, E. Coyle, and O. Wasynczuk, "Observing the power grid: Working toward a more intelligent, efficient, and reliable smart grid with increasing user visibility," *IEEE Signal Processing Magazine*, vol. 29, no. 5, pp. 24–32, Sept. 2012.

[3] A. Phadke and J. Thorp, *Synchronized phasor measurements and their applications*. Springer Science & Business Media, 2008.

[4] F. Li, W. Qiao, H. Sun, H. Wan, J. Wang, Y. Xia, Z. Xu, and P. Zhang, "Smart transmission grid: Vision and framework," *IEEE Transactions on Smart Grid*, vol. 1, no. 2, pp. 168–177, Sept. 2010.

[5] J. De La Ree, V. Centeno, J. S. Thorp, and A. G. Phadke, "Synchronized phasor measurement applications in power systems," *IEEE Transactions on Smart Grid*, vol. 1, no. 1, pp. 20–27, June 2010.

[6] F. Aminifar, M. Fotuhi-Firuzabad, A. Safdarian, A. Davoudi, and M. Shahidehpour, "Synchrophasor measurement technology in power systems: Panorama and state-of-the-art," *IEEE Access*, vol. 2, pp. 1607–1628, Jan. 2015.

[7] Y. Xia, S. Kanna, and D. P. Mandic, "Maximum likelihood parameter estimation of unbalanced three-phase power signals," *IEEE Transactions on Instrumentation and Measurement*, vol. 67, no. 3, pp. 569–581, Mar. 2018.

[8] L. Zhan, Y. Liu, and Y. Liu, "A Clarke Ttransformation-based DFT Phasor and Frequency Algorithm for wide frequency range," *IEEE Transactions on Smart Grid*, vol. 9, no. 1, pp. 67 – 77, Jan. 2018.

[9] H. Wen, C. Li, and W. Yao, "Power system frequency estimation of sine-wave corrupted with noise by windowed three-point interpolated dft," *IEEE Transactions on Smart Grid*, vol. 9, no. 5, pp. 5163–5172, Sept. 2018.

[10] V. Choqueuse, A. Belouchrani, F. Auger, and M. Benbouzid, "Frequency and phasor estimations in three-phase systems: Maximum likelihood algorithms and theoretical performance," *IEEE Transactions on Smart Grid (Accepted for Publication)*, pp. 1–1, 2018.

[11] S. Vejdan, M. Sanaye-Pasand, and O. P. Malik, "Accurate dynamic phasor estimation based on the signal model under off-nominal frequency and oscillations," *IEEE Transactions on Smart Grid*, vol. 8, no. 2, pp. 708–719, Mar. 2017.

[12] L. Fu, J. Zhang, S. Xiong, Z. He, and R. Mai, "A modified dynamic synchrophasor estimation algorithm considering frequency deviation," *IEEE Transactions on Smart Grid*, vol. 8, no. 2, pp. 640–650, Mar. 2017.

[13] D. Rife and R. Boorstyn, "Single tone parameter estimation from discrete-time observations," *IEEE Transactions on Information Theory*, vol. 20, no. 5, pp. 591–598, Sep 1974.

[14] P. Stoica and R. Moses, *Introduction to spectral analysis*. Prentice hall New Jersey:, 1997, vol. 1.

[15] D. Agrez, "Weighted multipoint interpolated DFT to improve amplitude estimation of multifrequency signal," *IEEE Transactions on Instrumentation and Measurement*, vol. 51, no. 2, pp. 287–292, Apr. 2002.

[16] D. Belega and D. Petri, "Accuracy analysis of the multicycle synchrophasor estimator provided by the interpolated DFT algorithm," *IEEE Transactions on Instrumentation and Measurement*, vol. 62, no. 5, pp. 942–953, May 2013.

[17] P. Romano and M. Paolone, "Enhanced interpolated-DFT for synchrophasor estimation in FPGAs: Theory, implementation, and validation of a PMU prototype," *IEEE Transactions on Instrumentation and Measurement*, vol. 63, no. 12, pp. 2824–2836, Dec. 2014.

[18] D. Macii, D. Fontanelli, G. Barchi, and D. Petri, "Impact of acquisition wideband noise on synchrophasor measurements: A design perspective," *IEEE Transactions on Instrumentation and Measurement*, vol. 65, no. 10, pp. 2244–2253, Oct. 2016.

[19] E. Clarke, *Circuit analysis of AC power systems*. Wiley, 1943, vol. 1.

[20] G. C. Paap, "Symmetrical components in the time domain and their application to power network calculations," *IEEE Transactions on Power Systems*, vol. 15, no. 2, pp. 522–528, May 2000.

[21] A. Pradhan, A. Routray, and A. Basak, "Power system frequency estimation using least mean square technique," *IEEE Transactions on Power Delivery*, vol. 20, no. 3, pp. 1812–1816, July 2005.

[22] Y. Xia, S. C. Douglas, and D. P. Mandic, "Adaptive frequency estimation in smart grid applications: Exploiting noncircularity and widely linear adaptive estimators," *IEEE Signal Processing Magazine*, vol. 29, no. 5, pp. 44–54, Sept. 2012.

[23] V. Choqueuse, M. Benbouzid, Y. Amirat, and S. Turri, "Diagnosis of three-phase electrical machines using multidimensional demodulation techniques," *IEEE Transactions on Industrial Electronics*, vol. 59, no. 4, pp. 2014–2023, Apr. 2012.

[24] Y. Chen and H. C. So, "Accurate parameter estimation for unbalanced three-phase system," *The Scientific World Journal*, vol. 2014, Aug 2014.

[25] V. Choqueuse, E. Elbouchikhi, and M. Benbouzid, "Maximum likelihood frequency estimation in smart grid applications," in *24th International Symposium on Industrial Electronics (ISIE 2015)*. Buzios, Brazil: IEEE, 2015, pp. 1339 – 1344.

[26] I. Jolliffe, *Principal component analysis*. Wiley Online Library, 2002.

[27] A. Von Jouanne and B. Banerjee, "Assessment of voltage unbalance," *IEEE transactions on power delivery*, vol. 16, no. 4, pp. 782–790, Oct. 2001.

[28] V. Ignatova, P. Granjon, and S. Bacha, "Space vector method for voltage dips and swells analysis," *IEEE Transactions on Power Delivery*, vol. 24, no. 4, pp. 2054–2061, Oct. 2009.

[29] M. Sun, S. Demirtas, and Z. Sahinoglu, "Joint voltage and phase unbalance detector for three phase power systems," *Signal Processing Letters, IEEE*, vol. 20, no. 1, pp. 11–14, Jan. 2013.

[30] T. Routtenberg, R. Concepcion, and L. Tong, "PMU-based detection of voltage imbalances with tolerance constraints," *IEEE Transactions on Power Delivery*, vol. 32, no. 1, pp. 484–494, Feb. 2017.

[31] Z. Oubrahim, V. Choqueuse, Y. Amirat, and M. Benbouzid, ""disturbances classification based on a model order selection method for power quality monitoring"," *IEEE Transactions on Industrial Electronics*, Dec. 2017.

[32] T. Routtenberg and Y. C. Eldar, "Centralized identification of imbalances in power networks with synchrophasor data," *IEEE Transactions on Power Systems*, vol. 33, no. 2, pp. 1981–1992, Mar. 2018.

[33] T. Routtenberg, Y. Xie, R. Willett, and L. Tong, "PMU-based detection of imbalance in three-phase power systems," *IEEE Transactions on Power Systems*, vol. 30, no. 4, pp. 1966–1976, July 2015.

[34] *IEEE Standard Definitions for the Measurement of Electric Power Quantities Under Sinusoidal, Nonsinusoidal, Balanced, or Unbalanced Conditions*. IEEE Std 1459-2010 (Revision of IEEE Std 1459-2000), Mar. 2010.

[35] A. V. Oppenheim, R. W. Schafer, J. R. Buck *et al.*, *Discrete-time signal processing*. Prentice-hall Englewood Cliffs, 1989, vol. 2.

[36] P. Granjon and G. S. L. Phua, "Estimation of geometric properties of three-component signals for system monitoring," *Mechanical Systems and Signal Processing*, vol. 97, pp. 95–111, Dec. 2017.

[37] S. M. Kay, "Fundamentals of statistical signal processing, vol. II: Detection theory," *Signal Processing. Upper Saddle River, NJ: Prentice Hall*, 1998.

[38] S. M. Kay, "Fundamentals of statistical processing, vol. I: Estimation theory," *Signal Processing. Upper Saddle River, NJ: Prentice Hall*, vol. 1, 1993.

[39] J. A. Nelder and R. Mead, "A simplex method for function minimization," *The computer journal*, vol. 7, no. 4, pp. 308–313, Jan. 1965.

[40] *IEEE Standard for Synchrophasor Measurements for Power Systems*. IEEE Std C37.118.1-2011 (Revision of IEEE Std C37.118-2005), Dec. 2011.

[41] R. Horn and C. Johnson, *Matrix analysis*. Cambridge university press, 2012.